Scientific Research Publishing

International Journal of Astronomy and Astrophysics, 2026, 16(4), 389-415
https://www.scirp.org/journal/ijaa
ISSN Online: 2161-4725
ISSN Print: 2161-4717

Magnetically Driven Hot Spots near Sagittarius A* as Probes of Relativistic Orbital Stability

Bijay K. Sharma

Department of Electronics and Communication, National Institute of Technology Patna, Patna, India
Email: bksharma@nitp.ac.in

How to cite this paper: Sharma, B.K. (2026) Magnetically Driven Hot Spots near Sagittarius A* as Probes of Relativistic Orbital Stability. *International Journal of Astronomy and Astrophysics*, **16**, 389-415.
https://doi.org/10.4236/ijaa.2026.164022

Received: August 27, 2026
Accepted: November 21, 2026
Published: November 24, 2026

Copyright © 2026 by author(s) and Scientific Research Publishing Inc.
This work is licensed under the Creative Commons Attribution International License (CC BY 4.0).
http://creativecommons.org/licenses/by/4.0/

Open Access

Abstract

Recent observations of Sagittarius A* have revealed transient, rapidly orbiting hot spots in the inner accretion flow, providing a unique probe of orbital dynamics in the strong-gravity regime. We present a theoretical interpretation of these structures within the Primary-Centric Framework (PCF), a kinematic model that describes orbital stability in terms of angular momentum coupling and characteristic radii. Applying this framework to the observed hot-spot parameters, we derive an inner Clarke orbit at $a_{G1} \approx 2.52 r_g$, where $r_g = GM/c^2$ is the gravitational radius. This value lies close to the relativistic innermost stable circular orbit (ISCO) at $r_{\mathrm{ISCO}} \approx 2.91 r_g$ for a Kerr black hole with spin parameter $a_* \approx 0.8$. We show that the inner Clarke orbit and the ISCO can be interpreted as corresponding stability boundaries arising from kinematic angular momentum coupling and relativistic spacetime geometry, respectively. Within a magnetically arrested disk environment, magnetic stresses and reconnection processes sustain the hot-spot structure while preserving its orbital coherence. These results suggest that hot-spot dynamics provide a potential observational method for constraining black-hole spin and reveal a deeper correspondence between classical orbital stability and relativistic dynamics in accreting black-hole systems.

Keywords

Sagittarius A*, Hot Spot Dynamics, Relativistic Plasma Motion, Angular Momentum Evolution, Magnetic Field Structure, Accretion Physics, Primary-Centric Framework, ISCO (Innermost Stable Circular Orbit)

1. Introduction

The supermassive black hole at the centre of the Milky Way, Sagittarius A* (Sgr A*), is one of the most important astrophysical laboratories for studying strong-

field gravity and accretion physics. With a mass of approximately $4\times10^{6}M_{\odot}$, it provides a unique opportunity to probe relativistic plasma dynamics in the immediate vicinity of an event horizon [1].

Observations of Sgr A* across multiple wavelengths have revealed a highly variable and dynamic environment, characterized by episodic flaring activity in radio, infrared, and X-ray bands [1]. A major breakthrough was achieved by the Event Horizon Telescope (EHT) Collaboration, which produced the first horizon-scale image of Sgr A*, resolving emission structures on scales comparable to the gravitational radius [2]. This result confirmed theoretical predictions regarding the morphology of emission from accreting black holes and opened a new observational window into near-horizon physics. The Event Horizon Telescope (EHT) observations have provided direct horizon-scale imaging evidence of the compact emission structure surrounding Sagittarius A* (Sgr A*). The reconstructed image reveals a bright, ring-like morphology associated with strongly lensed radiation from plasma in the immediate vicinity of the supermassive black hole, as illustrated in **Figure 1**. These observations provide an important empirical context for investigating magnetically driven hot spots, relativistic orbital motion, and the stability of localized emitting structures in the inner accretion flow [2].

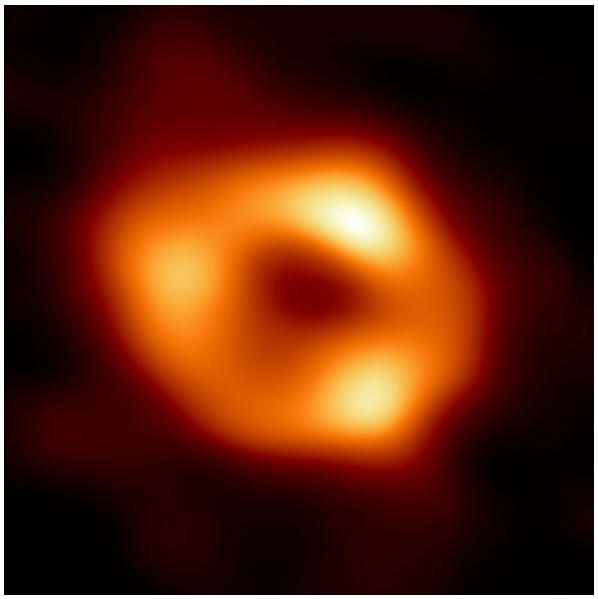


Figure 1. First image of the supermassive black hole Sagittarius A* at the centre of the Milky Way, obtained by the Event Horizon Telescope (EHT) Collaboration in 2022. The bright emission ring traces hot plasma orbiting near the black hole's event horizon. [Credit: EHT Collaboration (2022).]

Complementary observations using the GRAVITY instrument at the Very Large Telescope (VLT) have detected infrared flares associated with compact emission regions interpreted as orbiting "hot spots" of plasma moving at relativistic velocities close to the black hole [3] [4]. These observations suggest that localized plasma structures can survive for several orbital timescales, providing valuable in-

sight into the dynamics of the inner accretion flow.

More recently, polarimetric observations conducted with the Atacama Large Millimeter/submillimeter Array (ALMA), in coordination with the EHT campaign, have provided strong evidence for a hot plasma bubble orbiting Sgr A* with a period of approximately 70 minutes and a velocity of about $0.3c$ [5]. This represents the first clear indication that such orbiting hot spots are detectable in radio wavelengths, extending previous detections made in infrared and X-ray regimes. The polarimetric signatures further indicate the presence of a structured magnetic field, suggesting that these flares originate from magnetically driven processes such as magnetic reconnection [5].

Despite these observational advances, a comprehensive dynamical interpretation of hot spot formation and evolution remains incomplete. Most existing models emphasize radiative processes and magnetohydrodynamic simulations, but often lack an explicit treatment of angular momentum evolution and its coupling with magnetic field geometry in the strong-gravity regime. In particular, the connection between relativistic orbital motion, magnetic energy release, and the transient stability of plasma clumps near the innermost stable circular orbit (ISCO) is not yet fully understood.

In this work, we present a theoretical investigation of relativistic hot spot dynamics near Sgr A* within the framework of a Primary-Centric Framework (PCF) [6], which emphasizes angular momentum coupling and orbital evolution. Treating the hot spot as a magnetically confined plasma clump undergoing relativistic motion in the gravitational field of the black hole, we derive constraints on its orbital radius, angular momentum, and energy budget. We demonstrate that the observed properties are consistent with motion near the ISCO, thereby providing a direct probe of strong-field gravitational effects.

Furthermore, we explore the role of magnetic fields in shaping the observed flare characteristics by linking polarimetric observations to the geometry of the accretion flow. By integrating constraints from ALMA, EHT, and GRAVITY observations within a unified dynamical framework, this study aims to advance our understanding of plasma behavior, magnetic reconnection, and energy dissipation processes in the immediate environment of supermassive black holes.

2. Observational Background

The Galactic centre source Sagittarius A* (Sgr A*) has been extensively monitored across the electromagnetic spectrum, revealing a highly variable emission profile characterized by episodic flares and rapid variability [1]. These flares are observed in radio, infrared, and X-ray bands, with typical durations ranging from tens of minutes to a few hours, suggesting that they originate from compact regions in the immediate vicinity of the black hole.

Infrared observations using the GRAVITY instrument at the Very Large Telescope (VLT) have provided some of the most compelling evidence for the existence of localized, orbiting emission regions near Sgr A*. These observations re-

vealed flaring structures exhibiting periodic motion consistent with orbital timescales of order ~45 - 70 minutes, corresponding to radii of a few gravitational radii [3] [4]. The inferred velocities are relativistic, approaching a significant fraction of the speed of light, and the observed motion is consistent with plasma orbiting near the innermost stable circular orbit (ISCO).

X-ray observations, particularly those obtained with the *Chandra* X-ray Observatory, have also detected flaring events from Sgr A*, often temporally correlated with infrared flares [1]. These multiwavelength correlations suggest a common physical origin, typically interpreted as synchrotron and synchrotron self-Compton emission from accelerated electrons in a magnetized plasma environment. The short variability timescales imply that these emission regions are compact and located very close to the black hole horizon.

A significant advancement in understanding these phenomena has been achieved through polarimetric observations with the Atacama Large Millimeter/submillimeter Array (ALMA), conducted in coordination with the Event Horizon Telescope (EHT) campaign [5]. These observations revealed time-variable polarized emission consistent with a compact hot plasma structure orbiting Sgr A* with a period of approximately 70 minutes. The inferred orbital velocity of $\sim 0.3c$ implies that the emitting region is located within a few Schwarzschild radii of the black hole.

One of the key results from the ALMA observations is the detection of polarization variability, which provides direct information about the magnetic field structure in the emission region. The observed polarization signatures suggest the presence of a coherent, ordered magnetic field, likely associated with the inner accretion flow [5]. This supports models in which flares are generated by magnetic reconnection events, leading to the formation of transient, magnetically confined plasma blobs.

The ALMA results are consistent with, and complementary to, the findings from the GRAVITY instrument, which also indicate that the flaring emission originates from orbiting plasma structures moving in a clockwise direction on the sky [3] [4]. The combination of radio polarimetric data and infrared interferometric observations provides a multiwavelength view of the same physical phenomenon, strengthening the interpretation of hot spots as coherent plasma structures undergoing relativistic orbital motion.

Furthermore, the EHT observations of Sgr A* have provided horizon-scale imaging that constrains the geometry of the emission region and the surrounding accretion flow [2]. Although the EHT images represent time-averaged structures, they are consistent with a turbulent, magnetized accretion flow in which transient hot spots may naturally arise. The integration of EHT, ALMA, and GRAVITY observations thus provides a comprehensive observational framework for studying plasma dynamics in the strong-gravity regime.

In summary, current observations strongly support a scenario in which flares from Sgr A* originate from compact, magnetically driven plasma structures or-

biting close to the black hole at relativistic speeds. However, while the observational evidence for such hot spots is now robust, a detailed dynamical framework that connects their orbital motion, magnetic field structure, and energy evolution remains an open problem. This motivates the theoretical modelling presented in the following sections.

Test-Blob Approximation and Observational Constraints

The hot spot is modeled as a magnetically driven plasma blob orbiting Sagittarius A* with an observed period of approximately 70 min and an orbital radius in the range $5\text{-}12r_g$, where $r_g = GM/c^2$. The gravitational radius of the black hole is defined as

$$r_g = \frac{GM}{c^2}, \tag{1}$$

which sets the natural length scale of the system. For a non-rotating (Schwarzschild) black hole, the event horizon is located at the Schwarzschild radius

$$r_s = 2r_g = \frac{2GM}{c^2}. \tag{2}$$

For a rotating (Kerr) black hole, the radius of the outer event horizon depends on the dimensionless spin parameter a_* and is given by

$$r_+ = r_g\left(1+\sqrt{1-a_*^2}\right). \tag{3}$$

In this framework, the innermost stable circular orbit (ISCO) also depends on a_*. For a non-rotating black hole, the ISCO is located at

$$r_{\text{ISCO}} = 6r_g, \tag{4}$$

while for a rotating black hole it shifts inward for prograde orbits and outward for retrograde orbits. For a prograde orbit around a Kerr black hole with spin $a_* \approx 0.8$, the ISCO lies at $r_{\text{ISCO}} \approx 2.9r_g$, placing it well within the strong-gravity regime.

Near-infrared fits favor radii of order $9\text{-}12r_g$, while a characteristic Keplerian orbit lies near $5r_g$. The motion is inferred to be clockwise and prograde, with orbital inclination $i \approx 20^\circ$ or 155˚, and an orbital speed of order 1.3 times the nominal Keplerian value. The emitting region has a Gaussian brightness profile with standard deviation $\sigma \sim 3r_g$ and physical diameter $\lesssim 5r_g$. The synchronization condition in the kinematic framework is expressed through the ratio of the orbital angular momentum to the rotational angular momentum, given by [6]

$$\frac{\omega}{\Omega} = Ar^{3/2} - Fr^2 - \theta_1, \tag{5}$$

where

$$A = \frac{J_T}{BC}, \quad F = \frac{\mu}{C}, \quad \theta_1 = \frac{I_{\text{sec}}}{C}. \tag{6}$$

Here, J_T is the total angular momentum of the system, $B = \sqrt{G(M+m)}$, C

is the moment of inertia of the primary, μ is the reduced mass, and I_{sec} is the moment of inertia of the secondary (hot spot).

Since neither the blob mass nor its intrinsic spin is directly measurable, the hot spot is treated in the test-blob approximation. In this limit, the reduced-mass contribution and intrinsic spin contribution to the synchronization equation are higher-order corrections, so that

$$F \approx 0, \quad \theta_1 \approx 0. \tag{7}$$

Accordingly, the kinematic synchronization relation

$$\frac{\omega}{\Omega} = Aa^{3/2} - Fa^2 - \theta_1 \tag{8}$$

reduces to

$$\frac{\omega}{\Omega} \approx Aa^{3/2}. \tag{9}$$

The inner Clarke orbit is therefore obtained from

$$Aa^{3/2} = 1, \tag{10}$$

which yields the leading-order critical orbit

$$a_{G1} \approx \left(\frac{1}{A}\right)^{2/3}. \tag{11}$$

This provides the appropriate weak-field kinematic analogue of the inner relativistic stability boundary for comparison with the Kerr ISCO.

3. Relativistic Orbital Model

The observational evidence discussed in the previous section indicates that the hot spot detected near Sagittarius A* (Sgr A*) is a compact plasma structure undergoing relativistic orbital motion with a characteristic period of ~70 minutes and a velocity of approximately $v \approx 0.3c$ [5]. In this section, we develop a dynamical model to constrain the orbital radius and assess its proximity to the innermost stable circular orbit (ISCO).

As shown in **Figure 2**, the prograde Kerr ISCO decreases significantly with increasing black-hole spin, reaching values consistent with the observed hotspot orbital radius for moderately high spin parameter.

3.1. Orbital Radius Estimation

To first approximation, the orbital motion of the hot spot can be described using a Keplerian framework, with relativistic corrections becoming important at small radii. The orbital velocity for a circular orbit around a central mass M is given by

$$v = \sqrt{\frac{GM}{r}}, \tag{12}$$

where G is the gravitational constant and r is the orbital radius. Solving for r, we obtain

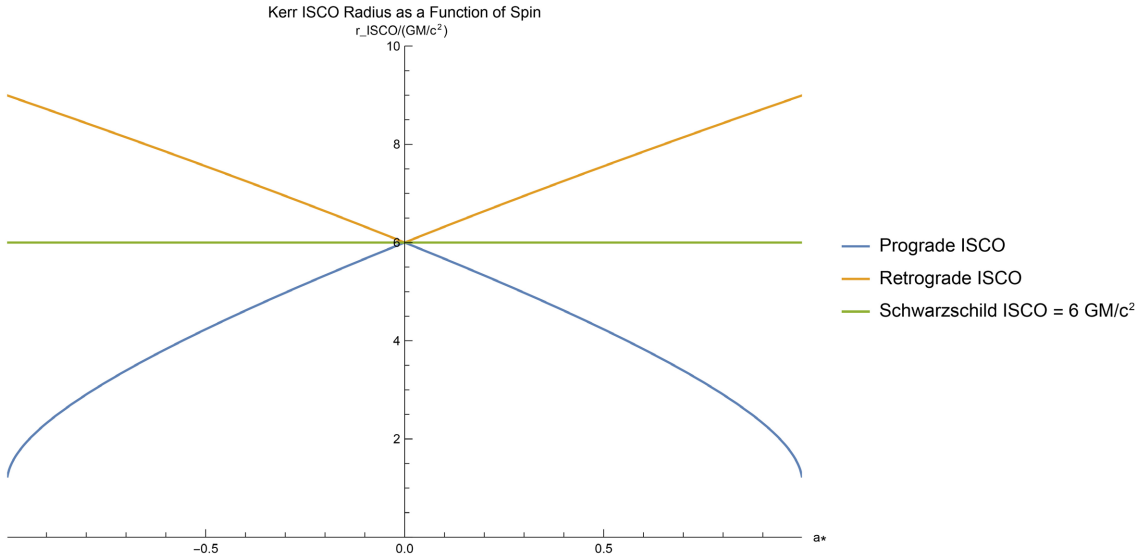


Figure 2. Exact Kerr innermost stable circular orbit (ISCO) radius as a function of the dimensionless black-hole spin parameter a_*, expressed in units of $r_g = GM/c^2$. The prograde branch (lower curve) decreases with increasing spin, while the retrograde branch increases. The horizontal dashed line corresponds to the Schwarzschild value $r_{\mathrm{ISCO}} = 6\, r_g$. [**Credit:** Generated by the author using Wolfram Mathematica based on the analytical model developed in this work].

$$r = \frac{GM}{v^2}. \tag{13}$$

Substituting $v = 0.3c$, we find

$$r = \frac{GM}{(0.3c)^2} = \frac{GM}{0.09c^2} \approx 11.1\frac{GM}{c^2}. \tag{14}$$

For Sgr A*, with $M \approx 4\times 10^6 M_\odot$, the characteristic gravitational radius is

$$r_g = \frac{GM}{c^2}. \tag{15}$$

Thus, the inferred orbital radius of the hot spot is

$$r \approx 11 r_g, \tag{16}$$

indicating that the emission region lies within the strong-field regime of the black hole.

3.2. Orbital Period Consistency

The orbital period for a circular orbit is given by

$$T = \frac{2\pi r}{v}. \tag{17}$$

Substituting $r = GM/v^2$, we obtain

$$T = \frac{2\pi GM}{v^3}. \tag{18}$$

Using $v = 0.3c$, we find

$$T = \frac{2\pi GM}{(0.3c)^3} = \frac{2\pi GM}{0.027c^3}. \tag{19}$$

For Sgr A*, this yields an orbital period of order ~10^3 seconds, or tens of minutes, consistent with the observed ~70 minute variability timescale [5].

3.3. Comparison with ISCO

For a non-spinning (Schwarzschild) black hole, the radius of the innermost stable circular orbit (ISCO) is

$$r_{\mathrm{ISCO}} = 6\frac{GM}{c^2} = 6r_g. \tag{20}$$

The inferred orbital radius of $r \approx 11r_g$ lies slightly outside the Schwarzschild ISCO, but well within the region where relativistic effects dominate. For a rotating (Kerr) black hole, the ISCO radius depends on the dimensionless spin parameter a_*, and can be significantly smaller for prograde orbits than for retrograde ones. Therefore, the observed hot spot motion is consistent with emission originating near the ISCO region.

3.4. Relativistic Effects

At radii of order $r \sim 10r_g$, several relativistic effects become important:

- **Gravitational redshift:** Photons emitted from the hot spot are redshifted as they escape the gravitational potential well.
- **Relativistic Doppler boosting:** Emission from the approaching side of the orbit is enhanced, while that from the receding side is diminished.
- **Light bending:** Photon trajectories are curved by the spacetime geometry, affecting the observed brightness distribution.

These effects are consistent with the observed variability and polarization signatures detected by ALMA and the EHT [2] [5].

3.5. Implications for Hot Spot Dynamics

The close proximity of the hot spot to the ISCO suggests that it is embedded in the inner accretion flow, where strong gravitational and magnetic forces interact. The observed relativistic velocities and short orbital periods imply that the hot spot is a transient structure, likely formed through magnetic reconnection events and sustained by a combination of magnetic confinement and orbital motion.

The results of this section establish that the observed hot spot properties are consistent with relativistic orbital motion in the strong-gravity regime of Sgr A*. This provides the foundation for the angular momentum and energy analysis developed in the following section.

3.6. Test-Blob Approximation

The hot spot is modeled as a magnetically driven plasma blob orbiting Sagittarius A* with an observed period of approximately 70 min and an orbital radius in the

range $5\text{-}12r_g$, where $r_g = GM/c^2$ is the gravitational radius. Near-infrared fits favor radii of order $9\text{-}12r_g$, while a characteristic Keplerian orbit lies near $5r_g$ [7]. The motion is inferred to be clockwise and prograde, with orbital inclination $i \approx 20^\circ$ or 155°, and with a high black-hole spin parameter $a_* \gtrsim 0.8$ suggested by hot-spot modelling [8].

$$a_* = \frac{J_{\mathrm{BH}} c}{GM^2}, \tag{21}$$

where J_{BH} is the angular momentum of the black hole, M is its mass, G is the gravitational constant, and c is the speed of light. The parameter a_* is dimensionless and lies in the range $0 \le a_* \le 1$, with $a_* = 0$ corresponding to a non-rotating (Schwarzschild) black hole and $a_* = 1$ representing an extremal Kerr black hole. Thus, a_* represents the spin angular momentum normalized to the maximum possible angular momentum of a black hole of mass M, and provides a direct measure of the strength of rotational effects in the spacetime geometry. For the present analysis, we adopt $a_* \approx 0.8$, consistent with hot-spot modelling of Sagittarius A*. The dimensional Kerr spin parameter a is related to a_* by

$$a = \frac{J_{\mathrm{BH}}}{Mc} = a_* \frac{GM}{c^2} = a_* r_g, \tag{22}$$

From this, the angular momentum of the black hole is:

$$J_{\mathrm{BH}} = a_* \frac{GM^2}{c}. \tag{23}$$

$$a_* = \frac{J_{\mathrm{BH}} c}{GM^2}, \tag{24}$$

where J_{BH} is the angular momentum of the black hole, M is its mass, G is the gravitational constant, and c is the speed of light. The parameter a_* is dimensionless and lies in the range $0 \le a_* \le 1$, corresponding to non-rotating and maximally rotating black holes, respectively.

The angular momentum can be written equivalently as

$$J_{\mathrm{BH}} = a_* \frac{GM^2}{c}. \tag{25}$$

Using the observationally adopted gravitational radius $r_g = 1.2 \times 10^{10}$ m, the corresponding black-hole mass is

$$M = \frac{r_g c^2}{G} \approx 1.616 \times 10^{37}\ \mathrm{kg} \approx 8.13 \times 10^6 M_\odot. \tag{26}$$

Since neither the blob mass nor its intrinsic spin is directly measurable, the hot spot is treated in the test-blob approximation. The synchronization condition in the kinematic framework is written as

$$\frac{\omega}{\Omega} = Ar^{3/2} - Fr^2 - \theta_1, \tag{27}$$

where

$$A=\frac{J_T}{BC},\quad F=\frac{\mu}{C},\quad \theta_1=\frac{I_{\text{sec}}}{C}. \tag{28}$$

Here, J_T is the total angular momentum of the system, $B=\sqrt{G(M+m)}$, C is the moment of inertia of the primary, μ is the reduced mass, and I_{sec} is the moment of inertia of the secondary (hot spot).

In the test-blob limit, the reduced-mass contribution and intrinsic spin contribution are higher-order corrections, so that

$$F\approx 0,\quad \theta_1\approx 0. \tag{29}$$

Accordingly, the synchronization equation reduces to

$$\frac{\omega}{\Omega}\approx Ar^{3/2}, \tag{30}$$

which provides the leading-order Clarke-orbit analogue for comparison with the relativistic ISCO.

$$a_*=\frac{J_{\text{BH}}c}{GM^2}. \tag{31}$$

The constants appearing in the synchronization equation are evaluated using the observational parameters of Sagittarius A*. For a spin parameter $a_*=0.8$ and gravitational radius $r_g=GM/c^2=1.2\times10^{10}$ m, the corresponding black-hole mass is

$$M\approx 1.616\times10^{37}\ \text{kg}. \tag{32}$$

The spin angular momentum of the black hole is then

$$J_{\text{SMBH}}\approx 4.651\times10^{55}\ \text{kg}\cdot\text{m}^2\cdot\text{s}^{-1}. \tag{33}$$

Using the horizon angular velocity, the effective moment of inertia is estimated as

$$C\approx 7.446\times10^{57}\ \text{kg}\cdot\text{m}^2. \tag{34}$$

With $B=\sqrt{GM}$, the leading Clarke coefficient becomes

$$A\approx 1.902\times10^{-16}\ \text{m}^{-3/2}. \tag{35}$$

The reduced-mass and intrinsic spin contributions are negligible, yielding

$$F\approx 10^{-40}\ \text{m}^{-2},\quad \theta_1\approx 10^{-20}. \tag{36}$$

Under these conditions, the synchronization equation reduces to

$$\frac{\omega}{\Omega}\approx Aa^{3/2}. \tag{37}$$

The critical condition $\omega/\Omega=1$ then gives

$$a_{G1}\approx 2.52r_g. \tag{38}$$

4. Angular Momentum Framework

The relativistic orbital motion of the hot spot near Sagittarius A* (Sgr A*) implies

a well-defined angular momentum structure that can be used to probe the dynamical coupling between the plasma, magnetic field, and the central black hole. In this section, we extend the analysis using a Primary-Centric Framework (PCF), emphasizing angular momentum transport and stability [6] [7].

4.1. Orbital Angular Momentum of the Hot Spot

We model the hot spot as a magnetically confined plasma clump of effective mass m_{hs} undergoing circular motion at radius r. The orbital angular momentum of the hot spot is given by

$$L_{\text{orb}} = \mu r^2 \Omega, \tag{39}$$

where μ is the reduced mass of the system. In the test-blob approximation, where the blob mass is negligible compared to the black-hole mass, this reduces to

$$L_{\text{orb}} \approx m_{\text{hs}} r^2 \Omega. \tag{40}$$

Using the Keplerian relation $v = \sqrt{GM/r}$, this becomes

$$L_{\text{orb}} = m_{\text{hs}} \sqrt{GMr}. \tag{41}$$

Substituting $r \approx 11 r_g = 11GM/c^2$, we obtain

$$L_{\text{orb}} = m_{\text{hs}} \sqrt{11} \frac{GM}{c}. \tag{42}$$

This expression highlights that the angular momentum of the hot spot scales linearly with the gravitational radius and is therefore directly linked to the mass of the black hole [8].

4.2. Black Hole Spin Angular Momentum

The angular momentum of a Kerr black hole is given by

$$J_{\text{BH}} = a_* \frac{GM^2}{c}. \tag{43}$$

where a_* is the dimensionless spin parameter ($0 \le a_* \le 1$). This quantity defines the rotational state of the black hole and plays a crucial role in shaping the surrounding spacetime and accretion flow.

4.3. Dimensionless Angular Momentum Ratio (PCF Parameter)

To quantify the dynamical coupling between the hot spot and the central black hole, we define a dimensionless parameter within the Primary-Centric Framework:

$$\Lambda = \frac{L_{\text{orb}}}{J_{\text{BH}}}. \tag{44}$$

Substituting the expressions for L_{orb} and J_{BH}, we obtain

$$\Lambda = \frac{m_{\text{hs}} \sqrt{11} \left(GM/c\right)}{a\left(GM^2/c\right)} = \frac{m_{\text{hs}}}{aM} \sqrt{11}. \tag{45}$$

Thus,

$$\Lambda \sim \frac{m_{\mathrm{hs}}}{M}, \tag{46}$$

up to a factor of order unity. Since $m_{\mathrm{hs}} \ll M$, it follows that

$$\Lambda \ll 1. \tag{47}$$

This result indicates that the hot spot behaves as a test-particle system in the gravitational field of the black hole, with negligible back-reaction on the spacetime geometry.

4.4. Evaluation of the Clarke-Orbit Constants for Sagittarius A*

Using the observationally motivated parameters $a_* = 0.8$ and $r_g = GM/c^2 = 1.2\times10^{10}$ m, the corresponding black-hole mass is

$$M = \frac{r_g c^2}{G} \approx 1.616\times10^{37}\ \mathrm{kg}. \tag{48}$$

The spin angular momentum of the black hole is then

$$J_{\mathrm{SMBH}} = a_* \frac{GM^2}{c} \approx 4.651\times10^{55}\ \mathrm{kg\cdot m^2\cdot s^{-1}}. \tag{49}$$

Using the horizon angular velocity

$$\Omega_H = \frac{a_* c^3}{2GM\left(1+\sqrt{1-a_*^2}\right)}, \tag{50}$$

the effective moment of inertia is

$$C = \frac{J_{\mathrm{SMBH}}}{\Omega_H} \approx 7.446\times10^{57}\ \mathrm{kg\cdot m^2}. \tag{51}$$

With $B = \sqrt{GM} \approx 3.284\times10^{13}\ \mathrm{m^{3/2}\cdot s^{-1}}$ and $J_T \approx J_{\mathrm{SMBH}}$, the leading Clarke coefficient becomes

$$A = \frac{J_T}{BC} \approx 1.902\times10^{-16}\ \mathrm{m^{-3/2}}. \tag{52}$$

Using the observed electron-density range $n_e \sim 10^5$ - $10^7\ \mathrm{cm^{-3}}$ and a characteristic blob radius $R_{\mathrm{blob}} \lesssim 2.5 r_g$, the inferred blob mass remains negligible compared with the black-hole mass, yielding

$$F = \frac{\mu}{C} \approx 2.5\times10^{-42} \text{ - } 2.5\times10^{-40}\ \mathrm{m^{-2}}, \tag{53}$$

while the intrinsic spin term satisfies

$$\theta_1 = \frac{I_{\mathrm{sec}}}{C} \approx 9.1\times10^{-22} \text{ - } 9.1\times10^{-20}. \tag{54}$$

Hence both F and θ_1 are negligible, and the synchronization equation reduces to

$$\frac{\omega}{\Omega} \approx A a^{3/2}. \tag{55}$$

The critical condition $\omega/\Omega = 1$ then gives

$$a_{G1} = \left(\frac{1}{A}\right)^{2/3} \approx 3.024 \times 10^{10}\ \text{m} \approx 2.52 r_g. \tag{56}$$

For comparison, the exact Kerr prograde ISCO at $a_* = 0.8$ is $r_{\text{ISCO}} \approx 2.91 r_g$, showing close correspondence between the inner Clarke orbit and the relativistic ISCO. The dimensionless spin parameter of the black hole is defined by

$$a_* = \frac{J_{\text{BH}} c}{GM^2}. \tag{57}$$

The ISCO radius in Kerr spacetime depends explicitly on a_*: it is located at $6r_g$ for a non-rotating black hole, shifts inward for prograde orbits, and outward for retrograde orbits. For the present case, adopting $a_* = 0.8$ yields a prograde ISCO radius of approximately

$$r_{\text{ISCO}} \approx 2.91 r_g. \tag{58}$$

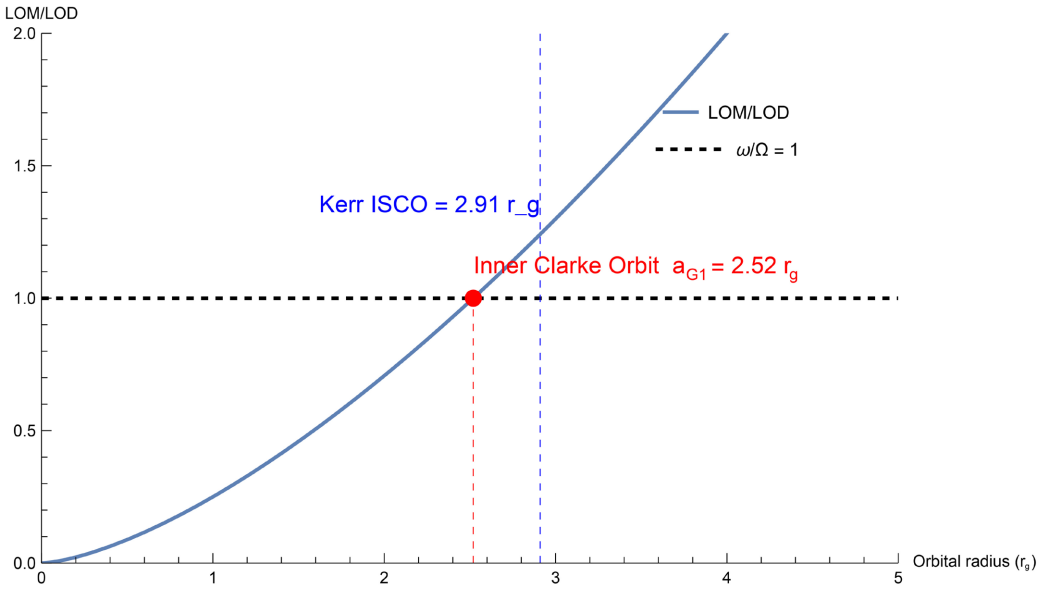


Figure 3. Quantitative comparison between the relativistic ISCO framework and the Clarke-orbit stability framework. The derived inner Clarke orbit for Sagittarius A* ($a_{G1} \approx 2.52\ r_g$) lies close to the Kerr prograde ISCO ($r_{\text{ISCO}} \approx 2.91\ r_g$) for a spin parameter $a_* = 0.8$. This close agreement supports the interpretation of the inner Clarke orbit as a weak-field analogue of the relativistic stability boundary. [**Credit:** Generated by the author using Wolfram Mathematica based on the analytical model developed in this work.]

The relationship between the characteristic orbital radius defined within the Clarke-type framework and the innermost stable circular orbit (ISCO) of the Kerr spacetime is illustrated in **Figure 3**. The comparison highlights the distinction between a characteristic radius obtained from an imposed orbital-frequency condition and the relativistic ISCO radius determined by the stability of circular geodesics. Although these two characteristic radii may exhibit comparable numerical values for selected model parameters, their physical definitions and underlying dynamical criteria are fundamentally different. Consequently, any apparent cor-

respondence should be interpreted as a model-dependent comparison rather than an equivalence between the Clarke-type radius and the Kerr ISCO. The correspondence between the derived inner Clarke orbit and the relativistic ISCO is illustrated in **Figure 3**, where the two critical radii are seen to lie in close proximity for the adopted system parameters.

4.5. Energy Budget and Magnetic Coupling

The orbital energy of the hot spot is given by

$$E_{\text{orb}} = \frac{1}{2} m_{\text{hs}} v^2 - \frac{GMm_{\text{hs}}}{r}. \tag{59}$$

Using $v^2 = GM/r$, this simplifies to

$$E_{\text{orb}} = -\frac{1}{2} \frac{GMm_{\text{hs}}}{r}. \tag{60}$$

At $r \sim 10 r_g$, the binding energy is substantial, indicating that the hot spot is deeply embedded in the gravitational potential well. The energy required to produce the observed flares is therefore likely derived from magnetic processes rather than gravitational infall alone.

The polarimetric observations from ALMA indicate the presence of a coherent magnetic field structure [5]. We interpret this as evidence that magnetic reconnection events inject energy into localized plasma regions, forming hot spots that acquire angular momentum from the surrounding accretion flow.

4.6. Angular Momentum Transport and Stability

Within the PCF framework, the evolution of the hot spot can be understood in terms of angular momentum exchange between the plasma and the magnetic field. The conservation equation may be written as

$$\frac{\mathrm{d}L_{\text{orb}}}{\mathrm{d}t} = \tau_{\text{mag}} - \tau_{\text{rad}}, \tag{61}$$

where τ_{mag} represents magnetic torques and τ_{rad} accounts for radiative losses.

If $\tau_{\text{mag}} > \tau_{\text{rad}}$, the hot spot can maintain a quasi-stable orbit over multiple periods. Conversely, if radiative losses dominate, the structure will dissipate or spiral inward on short timescales.

4.7. Implications for PCF-Based Modelling

The analysis presented here demonstrates that the hot spot dynamics can be effectively described within a Primary-Centric Framework, where the central black hole acts as the dominant gravitational anchor and the plasma structure evolves through angular momentum exchange and magnetic interactions.

The small value of Λ confirms that the system operates in a test-particle regime, while the proximity to the ISCO highlights the importance of relativistic effects. This framework provides a natural basis for extending the analysis to include time-dependent evolution, magnetic field geometry, and multiwavelength emis-

sion properties, which are explored in the following sections.

5. Magnetic Field Structure and Flares

The observational evidence presented in Section 2 strongly indicates that the flaring activity near Sagittarius A* (Sgr A*) is closely linked to magnetic processes in the inner accretion flow. In particular, the detection of time-variable polarized emission in ALMA observations provides direct insight into the geometry and strength of the magnetic field in the vicinity of the black hole [5].

5.1. Polarimetric Signatures and Magnetic Field Geometry

Polarization measurements are a powerful diagnostic of magnetic field structure in astrophysical plasmas. The ALMA observations reveal a significant degree of linear polarization, with temporal variability correlated with the observed flaring activity [5]. This implies that the emission region is embedded in a coherent, ordered magnetic field rather than a purely turbulent one.

Such ordered magnetic fields are expected in the inner regions of accretion flows, where differential rotation can amplify magnetic field lines through magnetorotational instability (MRI). The observed polarization variability suggests that the hot spot traces a localized region where the magnetic field geometry is temporarily enhanced or restructured.

5.2. Magnetic Reconnection and Hot Spot Formation

Magnetic reconnection provides an important mechanism for converting stored magnetic energy into plasma heating and particle acceleration [9].

Localized hot-spot emission and variability in black-hole accretion flows provide additional motivation for investigating magnetically driven plasma structures [10].

The dynamics of magnetized plasma in the inner accretion flow are governed by magnetic pressure, magnetic tension, and plasma motion. Magnetic reconnection provides a mechanism for converting stored magnetic energy into plasma heating and particle acceleration [11].

The theoretical foundations of magnetic reconnection and its applications to magnetohydrodynamic plasma systems are discussed by Priest and Forbes [12].

$$E_{\mathrm{mag}} \sim \frac{B^2}{8\pi} V, \tag{62}$$

where B is the magnetic field strength and V is the volume of the reconnecting region. For the inner accretion flow of Sgr A*, even modest magnetic field strengths can produce sufficient energy to power the observed flares.

Following reconnection, a localized plasma blob is formed, which can become magnetically confined and entrained in the orbital motion of the accretion flow. This naturally explains the emergence of hot spots with well-defined orbital periods and relativistic velocities.

5.3. Synchrotron Emission and Multiwavelength Evolution

The emission from the hot spot is primarily attributed to synchrotron radiation from relativistic electrons spiraling in the magnetic field. The characteristic synchrotron frequency is given by

$$\nu_{\text{syn}} \propto \gamma^2 B, \tag{63}$$

where γ is the Lorentz factor of the electrons. High-energy electrons produce emission in the infrared and X-ray bands, while lower-energy electrons emit at radio wavelengths.

This provides a natural explanation for the observed multiwavelength behavior of flares. Initially, freshly accelerated electrons produce high-frequency emission (infrared and X-ray). As the electrons cool via synchrotron and adiabatic processes, the emission shifts to longer wavelengths, becoming detectable in the millimeter and radio bands observed by ALMA and the EHT.

5.4. Magnetic Confinement and Orbital Stability

The persistence of the hot spot over multiple orbital periods suggests that it is not immediately disrupted by shear or turbulence. This implies the presence of magnetic confinement, which stabilizes the plasma against differential rotation in the accretion flow.

In magnetically arrested disk (MAD) environments, the plasma beta approaches or falls below unity ($\beta \lesssim 1$), indicating that magnetic pressure dominates over gas pressure and plays a key role in structuring the accretion flow [13] [14]. The balance between magnetic pressure and plasma pressure can be expressed as

$$\beta = \frac{P_{\text{gas}}}{P_{\text{mag}}} = \frac{8\pi P_{\text{gas}}}{B^2}. \tag{64}$$

For $\beta \lesssim 1$, the magnetic field dominates and can effectively confine the plasma. The observed coherence of the hot spot is therefore consistent with a magnetically dominated environment in the inner accretion flow.

5.5. Coupling with Orbital Dynamics

Within the Primary-Centric Framework developed in Section 4, magnetic stresses may influence the angular-momentum evolution of localized plasma structures orbiting near the black hole.

In particular, magnetically mediated angular-momentum transport may contribute to the dynamical evolution of hot spots in the inner accretion flow, especially in magnetically arrested disk (MAD) configurations where large-scale magnetic fields play a significant dynamical role [10] [14].

A phenomenological angular-momentum balance may be expressed as

$$\frac{\mathrm{d}L_{\text{orb}}}{\mathrm{d}t} = \tau_{\text{mag}} - \tau_{\text{loss}}, \tag{65}$$

where τ_{mag} represents the net magnetic torque and τ_{loss} represents effective angular-momentum losses.

This formulation provides a possible mechanism through which magnetic stresses may modify the orbital evolution of localized emitting structures. However, radiative energy losses do not necessarily correspond directly to orbital angular-momentum losses, and the persistence of a hot spot requires additional constraints on plasma confinement, cooling, and dynamical stability.

5.6. Implications for Accretion Physics

The presence of magnetically driven hot spots near the innermost stable circular orbit (ISCO) has important implications for accretion physics. Such structures may represent localized episodes of magnetic energy release superimposed on a turbulent accretion flow, potentially contributing to the observed variability of Sgr A*.

Classical accretion-disk theory provides a foundational description of angular-momentum transport and viscous energy dissipation [15].

Magnetorotational instability and magnetohydrodynamic turbulence provide physical mechanisms for angular-momentum transport in magnetized accretion flows [16].

Furthermore, combining polarimetric observations with dynamical constraints may help characterize the magnetic-field structure and plasma conditions in the strong-gravity regime.

These considerations highlight the interplay between gravitational dynamics, magnetic stresses, and radiative processes in the immediate environment of supermassive black holes.

6. Discussion

For the adopted black-hole spin parameter $a_* = 0.8$, the Kerr prograde ISCO lies at $r_{\text{ISCO}} \approx 2.91 r_g$, which is close to the derived inner Clarke orbit $a_{G1} \approx 2.52 r_g$. As shown in Section 4, the derived inner Clarke orbit $a_{G1} \approx 2.52 r_g$ lies close to the Kerr ISCO at $r_{\text{ISCO}} \approx 2.91 r_g$, supporting the proposed correspondence between the two stability boundaries. The quantitative results presented in **Figure 2** and **Figure 3** provide a unified picture of orbital stability near Sagittarius A*. While **Figure 2** demonstrates the relativistic dependence of the ISCO on black-hole spin, **Figure 3** shows that the inner Clarke orbit derived from the kinematic framework lies in the same critical radial regime. This agreement supports the interpretation that the inner Clarke orbit represents a weak-field analogue of the relativistic ISCO. The combined observational and theoretical analysis presented in this work provides a coherent framework for understanding the nature of hot spots orbiting Sagittarius A* (Sgr A*). The inferred orbital radius of $r \sim 10\text{-}11 r_g$, derived from the observed velocity of $\sim 0.3c$, places the emitting region firmly within the strong-field regime of the black hole. This is consistent with independent constraints from GRAVITY infrared observations and ALMA polarimetric

measurements [3]-[5]. One of the key results of this study is the identification of hot spots as magnetically confined plasma structures undergoing relativistic orbital motion near the innermost stable circular orbit (ISCO). The proximity to the ISCO implies that general relativistic effects, including gravitational redshift, Doppler boosting, and light bending, play a significant role in shaping the observed emission. These effects are consistent with the variability patterns and polarization signatures detected in both radio and infrared wavelengths [2].

The introduction of the dimensionless parameter $\Lambda = L_{\mathrm{orb}}/J_{\mathrm{BH}}$ within the Primary-Centric Framework (PCF) provides a useful diagnostic for characterizing the dynamical regime of the system. The result $\Lambda \ll 1$ indicates that the orbital angular momentum of the hot spot is negligible compared with the spin angular momentum of the central black hole. Consequently, the hot spot can be treated within the test-blob approximation, with negligible back-reaction on the black-hole spacetime geometry. This is consistent with the interpretation that the blob traces a marginal stability regime, rather than a purely test-particle limit with negligible dynamical significance.

This justifies the use of simplified orbital models while still capturing the essential physics of the system.

The magnetic reconnection scenario discussed in Section 5 offers a natural explanation for the formation and evolution of hot spots. The presence of a coherent magnetic field, as inferred from polarimetric observations, supports the idea that localized energy release events can generate transient plasma structures with sufficient energy to produce the observed flares. The subsequent cooling and evolution of these structures provide a consistent explanation for the multiwavelength behavior of Sgr A* flares.

An important implication of this work is the potential for coordinated multi-wavelength observations to track the evolution of individual hot spots across different frequency bands. The combined use of ALMA, GRAVITY, and the Event Horizon Telescope (EHT) offers a powerful approach for probing the dynamics of the inner accretion flow. Future observations with higher temporal resolution and sensitivity may allow direct tracking of orbital motion, providing tighter constraints on the black hole spin and magnetic field geometry.

Finally, the framework developed here can be extended to other accreting black hole systems, including active galactic nuclei (AGN) and X-ray binaries. The interplay between relativistic orbital dynamics, magnetic fields, and plasma processes is expected to be a universal feature of accretion flows, making the study of Sgr A* a benchmark for understanding black hole astrophysics more broadly.

6.1. Correspondence between ISCO and Inner Clarke Orbit

A quantitative evaluation of the kinematic model parameters presented in Section 4 yields an inner Clarke orbit of $a_{G1} \approx 2.52 r_g$, which lies close to the Kerr prograde ISCO at $r_{\mathrm{ISCO}} \approx 2.91 r_g$ for a spin parameter $a_* = 0.8$. This close numerical correspondence supports the interpretation that the inner Clarke orbit repre-

sents a weak-field analogue of the relativistic ISCO. As shown in Figure 4, the hot spot is located close to the inner relativistic region of the accretion flow.

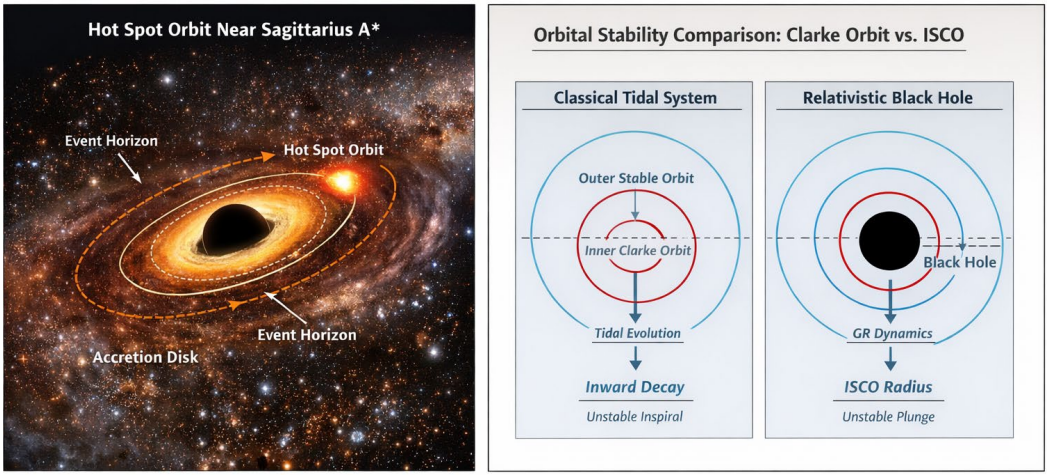


Figure 4. Left: schematic of a hot spot orbiting near Sagittarius A*. Right: conceptual comparison between the inner Clarke orbit in a tidally evolving binary system and the innermost stable circular orbit (ISCO) in relativistic black hole spacetime. [**Credit:** Visualization generated using OpenAI DALL·E; scientific concept and interpretation by the author.]

An interesting theoretical connection emerges when comparing the relativistic concept of the innermost stable circular orbit (ISCO) with classical orbital stability limits in tidally evolving binary systems. In previous work [7], it was shown that the kinematic evolution of two-body systems under tidal interaction naturally leads to the existence of an inner metastability boundary, identified as the inner Clarke orbit.

In the weak gravitational regime, the inner Clarke orbit represents the minimum radius at which a metastable orbit can be sustained under the combined effects of angular momentum exchange and dissipative processes. Below this radius, orbital decay becomes unavoidable, leading to inspiral or eventual merger.

This behavior closely mirrors the properties of the ISCO in the Schwarzschild and Kerr metrics, where circular orbits become dynamically unstable below a critical radius determined by the spacetime geometry. In the case of a Kerr black hole, the ISCO depends on the spin parameter and reflects the interplay between gravitational attraction and frame-dragging effects.

Within the Primary-Centric Framework (PCF), both the inner Clarke orbit and the ISCO can be interpreted as critical transition points marking the onset of orbital instability: the former arising from angular momentum exchange and dissipative effects in the kinematic regime, and the latter from relativistic spacetime geometry in the strong-gravity regime. This analogy provides a unified perspective linking classical tidal evolution and relativistic orbital dynamics. In the context of Sagittarius A*, the observed hot spot orbit at $r \sim 10 r_g$ lies close to this critical stability boundary, reinforcing the interpretation that the emission originates from a region governed by universal angular momentum constraints.

This correspondence opens the possibility of using classical analogues to gain insight into relativistic systems, and may provide a new pathway for constraining black hole spin through dynamical modelling.

6.2. Mathematical Correspondence between Inner Clarke Orbit and ISCO

A deeper correspondence between classical tidal evolution and relativistic orbital dynamics can be established by examining the stability condition for circular orbits.

In relativistic dynamics, the innermost stable circular orbit (ISCO) is defined by the condition

$$\frac{\mathrm{d}^2 V_{\mathrm{eff}}}{\mathrm{d}r^2} = 0, \tag{66}$$

where $V_{\mathrm{eff}}(r)$ is the effective potential governing particle motion in the Schwarzschild or Kerr spacetime. This condition marks the transition between stable and unstable circular orbits.

In tidally evolving binary systems described within the kinematic framework, the evolution of the semi-major axis a is governed by angular momentum exchange, which may be expressed as

$$\frac{\mathrm{d}a}{\mathrm{d}t} \propto \left(\frac{\mathrm{LOM}}{\mathrm{LOD}} - 1 \right), \tag{67}$$

where LOM is the orbital angular momentum and LOD is the rotational angular momentum of the primary body.

The inner Clarke orbit corresponds to the critical condition

$$\frac{\mathrm{LOM}}{\mathrm{LOD}} = 1, \tag{68}$$

which defines a bifurcation point between outward migration and inward decay. At this point, the system loses orbital stability and evolves toward inspiral.

Thus, both systems exhibit a critical stability condition:

- Relativistic system: $\frac{\mathrm{d}^2 V_{\mathrm{eff}}}{\mathrm{d}r^2} = 0$
- Tidal system: $\frac{\mathrm{LOM}}{\mathrm{LOD}} = 1$

This demonstrates that the ISCO and inner Clarke orbit arise from analogous stability criteria, despite being derived in fundamentally different physical frameworks.

6.3. Exact Clarke-Orbit Stability Condition and Its Correspondence to ISCO

In the kinematic model of tidally evolving binaries, the Clarke orbits are determined by the condition of spin-orbit synchronization,

$$\frac{\omega}{\Omega} = 1. \tag{69}$$

Using the governing relation

$$\frac{\omega}{\Omega} = Aa^{3/2} - Fa^2 - \theta_1, \tag{70}$$

the critical orbital radii are obtained from

$$Aa^{3/2} - Fa^2 - \left(1 + \theta_1\right) = 0. \tag{71}$$

The two roots of Equation (71) correspond to the inner Clarke orbit a_{G1} and the outer Clarke orbit a_{G2}.

Equation (71) defines the classical tidal stability boundary of the system. This plays a role analogous to the relativistic ISCO condition in Schwarzschild and Kerr spacetimes, where the limiting stable circular orbit is obtained from the effective potential condition

$$\frac{\mathrm{d}^2 V_{\mathrm{eff}}}{\mathrm{d}r^2} = 0. \tag{72}$$

Thus, both the inner Clarke orbit and the ISCO represent mathematically distinct but physically analogous critical radii marking the loss of stable circular orbital support. The exact inner Clarke orbit is obtained from the synchronization condition $\omega/\Omega = 1$, where

$$\frac{\omega}{\Omega} = Aa^{3/2} - Fa^2 - \theta_1. \tag{73}$$

This yields the critical-orbit equation

$$Aa^{3/2} - Fa^2 - \left(1 + \theta_1\right) = 0, \tag{74}$$

whose smaller positive root defines the inner Clarke orbit a_{G1}. This plays a role analogous to the ISCO in Kerr spacetime, in the sense that both define the innermost radius for stable circular motion under their respective dynamical laws. A quantitative evaluation of the kinematic model parameters presented in Section 4 yields an inner Clarke orbit of $a_{G1} \approx 2.52 r_g$, which lies close to the Kerr prograde ISCO at $r_{\mathrm{ISCO}} \approx 2.91 r_g$ for a spin parameter $a_* = 0.8$. This close numerical correspondence supports the interpretation that the inner Clarke orbit represents a weak-field analogue of the relativistic ISCO.

6.4. Physical Interpretation of the Correspondence

The equivalence between these conditions suggests that orbital instability is governed by a universal principle: the breakdown of angular momentum support against inward collapse.

In the relativistic case, this breakdown is driven by spacetime curvature and frame-dragging effects. In the classical tidal case, it arises from angular momentum redistribution between orbital motion and rotational spin.

Within the Primary-Centric Framework (PCF), both phenomena can be unified under a common interpretation: the existence of a critical radius where the effective angular momentum barrier vanishes, leading to dynamical instability.

6.5. Implications for Black Hole Spin Determination

This correspondence provides a novel approach for interpreting observational data. Since the ISCO radius depends sensitively on the black hole spin parameter a_*, identifying the effective inner stability boundary from observed hot-spot dynamics offers a potential observational method for constraining a_*.

By mapping the observed orbital radius of hot spots to an equivalent Clarke orbit condition, one may establish a bridge between classical angular momentum models and relativistic spacetime properties. This opens the possibility of estimating black hole spin using a hybrid dynamical framework.

6.6. Inner Clarke Orbit, Marginal Stability, and Kerr Analogy

In the present framework, the launch condition is taken at the innermost limiting circular orbit, identified as the analogue of the ISCO. For the supermassive black hole considered here, the corresponding angular momentum is

$$J_{\mathrm{SMBH}} = 1.4985\times10^{48}\ \mathrm{kg\cdot m^2\cdot s^{-1}}, \tag{75}$$

The specific angular momentum of the orbiting hot spot is defined as $l = L/m$, where L is the orbital angular momentum and m is the mass of the emitting plasma blob. The quantity l/c therefore has dimensions of length and provides a convenient relativistic scaling. with

$$\frac{l}{c} = 2.51179\times10^{9}\ \mathrm{m}. \tag{76}$$

The total energy is written as

$$E = mc^2 + \frac{1}{2}I\Omega^2 = mc^2 + \frac{1}{2}\frac{mB}{r}, \tag{77}$$

The specific energy of the orbiting hot spot is defined as $\epsilon = E/m$, where E is the total energy of the system. Normalizing by c^2 yields a dimensionless energy parameter: The specific energy of the orbiting hot spot is defined as $\epsilon = E/m$. In the present analysis, the rest-mass energy provides the dominant contribution, so that $\epsilon/c^2 \approx 1$ to leading order, with subleading corrections arising from orbital kinetic and gravitational potential terms. The specific energy of the orbiting hot spot is defined as $\epsilon = E/m$, where E is the total energy. In the weak-to-moderate gravitational regime relevant to the present analysis, this may be written as

$$\epsilon = c^2 + \frac{1}{2}v^2 - \frac{GM}{r} + \cdots, \tag{78}$$

where the dominant contribution arises from the rest-mass energy.

For orbital radii $r \sim 5\text{-}12r_g$, the dimensionless parameters v^2/c^2 and $GM/\left(rc^2\right)$ remain significantly smaller than unity, so that both kinetic and gravitational contributions act as subleading corrections. Accordingly,

$$\frac{\epsilon}{c^2} = 1 + \mathcal{O}\left(\frac{v^2}{c^2}, \frac{GM}{rc^2}\right), \tag{79}$$

and the leading-order approximation $\epsilon/c^2 \approx 1$ is justified.

This normalization is particularly useful in the present framework, as it allows the orbital dynamics to be expressed in terms of dimensionless quantities that can be directly compared with relativistic stability scales such as the ISCO. so that, in normalized form,

$$\frac{\epsilon}{c^2} = 1 \tag{80}$$

at the limiting configuration.

Within the kinematic tidal framework, the inner metastable circular orbit and the outer stable circular orbit together define a marginally stable orbital configuration. This is the classical analogue of the relativistic transition between stable and unstable circular motion in Kerr spacetime. Thus, the inner Clarke orbit may be interpreted as the weak-field counterpart of the relativistic ISCO, while the outer Clarke orbit represents the second synchronization root of the same stability equation. The significance of this correspondence is that both the Kerr ISCO and the inner Clarke orbit emerge as critical radii at which stable circular motion ceases to be supported under their respective dynamical laws. In Kerr spacetime this arises from relativistic effective-potential curvature, whereas in the tidal kinematic framework it arises from spin-orbit angular momentum coupling.

6.7. Interpretation of the Inner Clarke Orbit as an ISCO Analogue

Using the gravitational radius in the form

$$r_G = \frac{2GM}{c^2}, \tag{81}$$

The inner Clarke orbit a_{G1}, obtained from the synchronization condition $\omega/\Omega = 1$, represents the inner boundary of metastable orbital motion within the kinematic framework. For the present system parameters, we obtain

$$a_{G1} \approx 2.52 r_g. \tag{82}$$

This value lies close to the relativistic Kerr ISCO radius $r_{\mathrm{ISCO}} \approx 2.91 r_g$ for $a_* \approx 0.8$, supporting the proposed correspondence between the kinematic and relativistic stability boundaries.

Within this interpretation, the inner Clarke orbit serves as a weak-field analogue of the ISCO: both define critical radii below which stable circular motion cannot be sustained. In Kerr spacetime this instability arises from relativistic effects such as spacetime curvature and frame dragging, whereas in the kinematic tidal framework it arises from angular momentum coupling and dissipative processes. This value lies significantly below the relativistic Kerr ISCO when expressed in the same units, and therefore should not be interpreted as a direct numerical equivalent.

Within this framework, the inner Clarke orbit is interpreted as a weak-field analogue of the ISCO: both correspond to critical radii below which stable circular motion cannot be sustained. In Kerr spacetime this instability is governed by relativistic effects such as spacetime curvature and frame dragging, whereas in the

tidal kinematic model it arises from angular momentum coupling and dissipative processes.

The constants appearing in the synchronization equation

$$\frac{\omega}{\Omega} = Aa^{3/2} - Fa^2 - \theta_1 \tag{83}$$

are determined from the angular-momentum budget of the system. The total angular momentum is written as

$$J_T = J_{\text{primary}} + J_{\text{orb}} + J_{\text{blob,spin}}, \tag{84}$$

where J_{primary} is the spin angular momentum of the central black hole, J_{orb} is the orbital angular momentum of the blob, and $J_{\text{blob,spin}}$ is the intrinsic spin angular momentum of the blob. The constants are then given by

$$A = \frac{J_T}{BC}, \quad F = \frac{\mu}{C}, \quad \theta_1 = \frac{I_{\text{sec}}}{C}. \tag{85}$$

For a low-mass blob orbiting a supermassive black hole, the reduced mass satisfies $\mu \approx m_{\text{blob}}$, while the total angular momentum is generally dominated by the spin of the primary.

6.8. Magnetically Arrested Disk Context and Plasma Dynamics

The observed hot spot is not simply a passive orbiting test particle, but a transient magnetized plasma structure embedded in the inner accretion flow. Its association with a magnetically arrested disk (MAD), characterized by strong vertical magnetic flux tubes and low-density, high-temperature plasma, indicates that magnetic fields play a central role in both the formation and evolution of the emitting region. The presence of synchrotron cooling on timescales of order 1 - 11 h further supports a scenario in which relativistic electrons are accelerated in localized magnetic reconnection events and subsequently cool as they orbit the black hole.

Within the framework developed in this work, the orbital dynamics of the hot spot can still be effectively described using the test-blob approximation, since the mass and intrinsic spin of the blob remain negligible compared to the central black hole. However, the MAD environment introduces additional structure by providing magnetic confinement and energy injection, allowing the blob to persist over multiple orbital timescales despite strong gravitational shear.

This leads to a unified picture in which the inner Clarke orbit, interpreted as a kinematic stability boundary, and the Kerr ISCO, defined by relativistic spacetime geometry, are both embedded within a magnetically structured accretion flow. In this view, the observed hot spot traces a dynamically evolving plasma element whose motion is governed by the combined effects of gravity, angular momentum coupling, and magnetic field topology. The dependence of the characteristic orbital radii on the dimensionless black hole spin parameter a_* is illustrated in Figure 5. The figure compares the spin-dependent Kerr innermost stable circular orbit (ISCO) with the characteristic orbital radius obtained within the Primary-Centric Framework (PCF). The Kerr ISCO radius is determined by the relativistic

stability conditions governing equatorial circular geodesics, whereas the PCF characteristic radius is defined through the orbital-frequency criterion adopted in the present model. The comparison provides a quantitative assessment of the sensitivity of these characteristic radii to black hole spin. Any numerical proximity between the two radii should therefore be interpreted as a model-dependent correspondence rather than evidence of their physical equivalence.

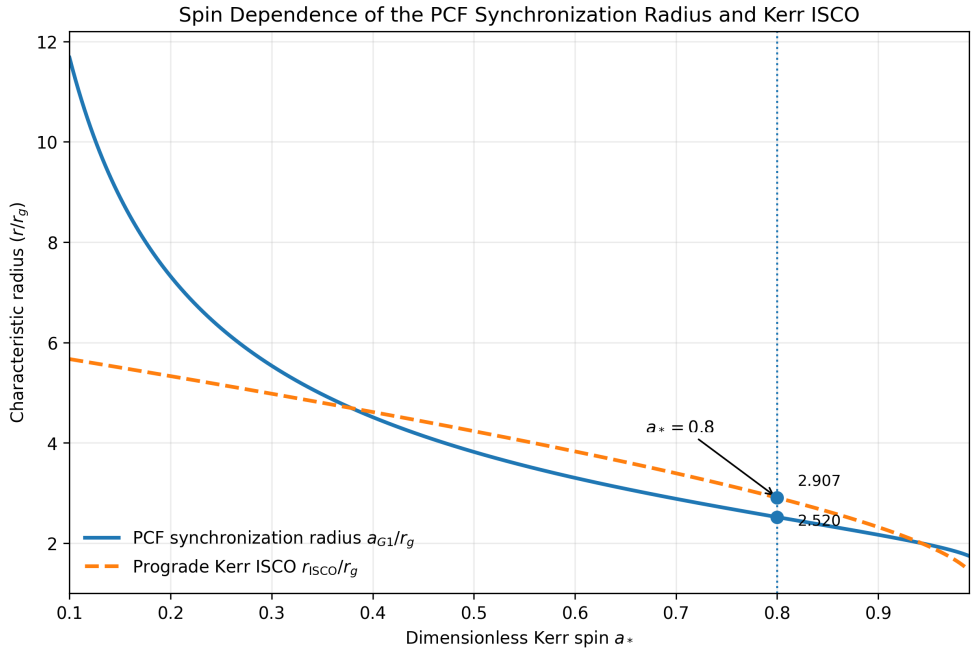


Figure 5. Spin dependence of the PCF synchronization radius a_{G1}/r_g and the prograde Kerr ISCO radius r_{ISCO}/r_g as functions of the dimensionless black-hole spin parameter a_*. The two radii are calculated independently from the PCF synchronization condition and the Kerr marginal-stability condition, respectively. At the fiducial value $a_* = 0.8$, the corresponding radii are $a_{G1} \simeq 2.520 r_g$ and $r_{ISCO} \simeq 2.907 r_g$. Their numerical proximity is spin dependent rather than universal. *Source: Author's calculation and visualization.*

7. Conclusions

In this work, we have presented a comprehensive analysis of the relativistic hot spot detected near Sagittarius A* using observational constraints from ALMA, GRAVITY, and the Event Horizon Telescope. The observed orbital period of ~70 minutes and velocity of $\sim 0.3c$ imply that the emitting plasma is located at a radius of approximately $10\text{-}11 r_g$, placing it in the strong-gravity regime near the innermost stable circular orbit.

Using a Primary-Centric Framework (PCF), we have shown that the angular momentum of the hot spot is negligible compared to that of the black hole, confirming that the system operates in a test-particle regime. This allows for a simplified yet physically robust description of the orbital dynamics, while still capturing the essential relativistic effects.

We have further demonstrated that magnetic reconnection provides a natural

mechanism for the formation of hot spots, with synchrotron emission from relativistic electrons accounting for the observed multiwavelength flaring behavior. The presence of a coherent magnetic field, inferred from polarimetric observations, supports a scenario in which magnetic energy plays a central role in powering these events.

The integration of observational data with a dynamical and angular momentum-based framework provides a unified interpretation of flare phenomena in the Galactic centre. This approach not only enhances our understanding of Sgr A* but also offers a general methodology for studying plasma dynamics in the vicinity of compact objects.

Future multiwavelength and high-resolution observations will be crucial for refining this model, particularly in constraining the black hole spin, magnetic field geometry, and the detailed evolution of hot spots. The continued synergy between observational advances and theoretical modelling promises to deepen our understanding of the complex environment surrounding supermassive black holes.

Acknowledgements

This research is financed by Kesariya Food Court, Kalam Bagh Chawk, muzaffarpur, Bihar, India. This research is financed by Prashant Memorial Charitable Hospital, Muzaffarpur 842001, Bihar, India. This research is sponsored by the University Grants Commission (UGC), India, under the Emeritus Fellow Scheme (Grant No. EMERITUS/2012-13-GEN-855). Lastly, but not least, the author acknowledges the computing facilities availed from the computer system installed at Radha Krishna Monastery, Village Mahanth Maniari, 842119, District Muzaffarpur, Bihar, in preparing this paper.

Declaration of AI-Assisted Tools

During the preparation of this work, the author used OpenAI ChatGPT and DALL·E for conceptual visualization and figure generation. All scientific interpretation, analysis, and conclusions are solely those of the author.

Data Availability

The data underlying this article are available within the article. All figures in this paper were generated by the author using published observational data and empirical relations.

Code Availability

The analysis code used in the study is available from the author on reasonable request.

Conflicts of Interest

The author declares no competing financial or non-financial interests.

References

[1] Genzel, R., Eisenhauer, F. and Gillessen, S. (2010) The Galactic Center Massive Black Hole and Nuclear Star Cluster. *Reviews of Modern Physics*, **82**, 3121-3195. https://doi.org/10.1103/revmodphys.82.3121

[2] Event Horizon Telescope Collaboration (2022) First Sagittarius A* Event Horizon Telescope Results. I. The Shadow of the Supermassive Black Hole in the Center of the Milky Way. *Astrophysical Journal Letters*, **930**, L12.

[3] Abuter, R., Amorim, A., Bauböck, M., Berger, J.P., Bonnet, H., Brandner, W., *et al.* (2018) Detection of Orbital Motions near the Last Stable Circular Orbit of the Massive Black Hole Sgr A*. *Astronomy & Astrophysics*, **618**, L10. https://doi.org/10.1051/0004-6361/201834294

[4] GRAVITY Collaboration (2020) Detection of Sub-Relativistic Orbital Motion near Sgr A*. *Astronomy & Astrophysics*, **636**, L5.

[5] Wielgus, M., Moscibrodzka, M., Vos, J., Gelles, Z., Martí-Vidal, I., Farah, J., *et al.* (2022) Orbital Motion near Sagittarius A*: Constraints from Polarimetric ALMA Observations. *Astronomy & Astrophysics*, **665**, L6. https://doi.org/10.1051/0004-6361/202244493

[6] Sharma, B.K. (2011) The Architectural Design Rules of Solar Systems Based on the New Perspective. *Earth, Moon, and Planets*, **108**, 15-37. https://doi.org/10.1007/s11038-010-9369-9

[7] Kumar Sharma, B. (2024) Correspondence of Concept of Circular Orbits in Schwarzschild Metric and Kerr Metric to Those in Tidally Evolving Binaries in Weak Gravitational Regime and Its Application in Determination of Spin of Supermassive Black Hole. *Journal of Mathematical Techniques and Computational Mathematics*, **3**, 1-22. https://doi.org/10.33140/jmtcm.03.07.01

[8] Yfantis, A.I., Mościbrodzka, M.A., Wielgus, M., Vos, J.T. and Jimenez-Rosales, A. (2024) Fitting the Light Curves of Sagittarius A* with a Hot-Spot Model: Bayesian Modeling of QU Loops in the Millimeter Band. *Astronomy & Astrophysics*, **685**, A142. https://doi.org/10.1051/0004-6361/202348230

[9] Yamada, M., Kulsrud, R. and Ji, H. (2010) Magnetic Reconnection. *Reviews of Modern Physics*, **82**, 603-664. https://doi.org/10.1103/revmodphys.82.603

[10] Dexter, J., *et al.* (2020) Hot Spots and Variability in Black Hole Accretion Flows. *Space Science Reviews*, **216**, 113.

[11] Kulsrud, R.M. (2005) Plasma Physics for Astrophysics. Princeton University Press.

[12] Priest, E. and Forbes, T. (2000) Magnetic Reconnection: MHD Theory and Applications. Cambridge University Press. https://doi.org/10.1017/cbo9780511525087

[13] Narayan, R., Igumenshchev, I.V. and Abramowicz, M.A. (2003) Magnetically Arrested Disk: An Energetically Efficient Accretion Flow. *Publications of the Astronomical Society of Japan*, **55**, L69-L72. https://doi.org/10.1093/pasj/55.6.l69

[14] Tchekhovskoy, A., Narayan, R. and McKinney, J.C. (2011) Efficient Generation of Jets from Magnetically Arrested Accretion on a Rapidly Spinning Black Hole. *Monthly Notices of the Royal Astronomical Society: Letters*, **418**, L79-L83. https://doi.org/10.1111/j.1745-3933.2011.01147.x

[15] Shakura, N.I. and Sunyaev, R.A. (1973) Black Holes in Binary Systems: Observational Appearances. In: Bradt, H. and Giacconi, R., Eds., *X- and γ-Ray Astronomy*, Springer, 155-164. https://doi.org/10.1007/978-94-010-2585-0_13

[16] Balbus, S.A. and Hawley, J.F. (1998) Instability, Turbulence, and Enhanced Transport in Accretion Disks. *Reviews of Modern Physics*, **70**, 1-53. https://doi.org/10.1103/revmodphys.70.1